The effect of orographic gravity waves on Antarctic polar stratospheric cloud occurrence and composition

S. P. Alexander,[1] A. R. Klekociuk,[1] M. C. Pitts,[2] A. J. McDonald,[3] and A. Arevalo-Torres[3]

[1]   A seasonal analysis of the relationship between mesoscale orographic gravity wave activity and polar stratospheric cloud (PSC) composition occurrence around the whole of Antarctica is presented. Gravity wave variances are derived from temperature measurements made with the Constellation Observing System for Meteorology, Ionosphere and Climate (COSMIC) Global Positioning System Radio Occultation (GPS-RO) satellites. Data from the Cloud-Aerosol Lidar with Orthogonal Polarization (CALIOP) instrument onboard the Cloud-Aerosol Lidar and Infrared Pathfinder Satellite Observations (CALIPSO) satellite are used to determine the PSC composition class distribution and spatial volume. The results show intermittent large wave activity above the Antarctic Peninsula which is coincident with large volumes of H_2O ice PSCs. These ice PSC volumes advect downstream, where increases in nitric acid trihydrate (NAT) PSC volumes occur, supporting the mountain wave seeding hypothesis. During winter 2007 in the latitude range 60°S–70°S, near the edge of the vortex and where temperatures are close to PSC formation thresholds, 30% of all PSCs are attributable to orographic gravity waves. In the separate composition classes, around 50% of both H_2O ice PSCs and a high NAT number density liquid–NAT mixture class of PSCs are due to these waves. While we show that planetary waves are the major determinant of PSC presence at temperatures close to the NAT formation threshold, we also demonstrate the important role of mesoscale, intermittent orographic gravity wave activity in accounting for the composition and distribution of PSCs around Antarctica.

Citation: Alexander, S. P., A. R. Klekociuk, M. C. Pitts, A. J. McDonald, and A. Arevalo-Torres (2011), The effect of orographic gravity waves on Antarctic polar stratospheric cloud occurrence and composition, *J. Geophys. Res.*, *116*, D06109, doi:10.1029/2010JD015184.

1.   Introduction

[2]   The important role of orographic gravity waves in the formation of Arctic polar stratospheric clouds (PSCs) and hence increasing ozone depletion has been recognized for some time [*Carslaw et al.*, 1998a, 1998b; *Dörnbrack et al.*, 2002; *Mann et al.*, 2005]. Evidence has been more recently presented indicating that some PSCs in the Antarctic are also formed through orographic gravity wave forcing [*Höpfner et al.*, 2006; *Eckermann et al.*, 2009]. Even if the synoptic-scale temperature is slightly too high, orographic waves allow the formation of H_2O ice PSCs via adiabatic cooling in their cool phases, which then seed the formation of nitric acid trihydrate (NAT) mother clouds [*Drdla et al.*, 2002; *Fueglistaler et al.*, 2002]. The areal coverage of the mountain wave induced H_2O ice PSCs is small and these quasi-stationary waves exist on relatively short time scales. Despite this, the strong eastward winds in the polar winter lower stratosphere mean that a significant amount of air flows through these clouds [*Carslaw et al.*, 1998a; *Cariolle et al.*, 1989]. Conversion of chlorine reservoirs into highly reactive (ozone-destroying) chlorine radicals occurs faster at lower temperatures. As PSCs enable nearly complete chlorine activation, the orographic mesoscale PSCs activate significant amounts of reactive forms of chlorine [*Carslaw et al.*, 1998a]. However, the difficulty in obtaining accurate mountain wave information in the polar vortices inhibits quantification of the effects of mountain wave induced NAT mother clouds [*World Meteorological Organization*, 2007].

[3]   The NAT mother cloud or NAT particles may advect isentropically significant distances downstream of the mountain wave source in a matter of hours or days [*Cariolle et al.*, 1989; *Carslaw et al.*, 1999; *Fueglistaler et al.*, 2003; *Höpfner et al.*, 2006]. PSC formation removes gas phase HNO_3 and the sedimentation of solid PSC particles results in dehydration and denitrification of the stratosphere during winter. This process prolongs polar ozone destruction by slowing the conversion of active chlorine back to reservoir species. A larger fraction of the total HNO_3 sediments out of

---

[1]Australian Antarctic Division, Kingston, Tasmania, Australia.
[2]NASA Langley Research Center, Hampton, Virginia, USA.
[3]Department of Physics and Astronomy, University of Canterbury, Christchurch, New Zealand.

the stratosphere over Antarctica than over the Arctic due to the more stable southern polar vortex [*Lowe and MacKenzie*, 2008].

[4] PSC formation also occurs during the cool phases of waves from nonorographic sources. Planetary waves create the necessary conditions via large-scale adiabatic cooling of air parcels to enable widespread PSC formation in latitude bands where background temperatures already hover close to their formation threshold. Using European Centre for Medium-Range Weather Forecasts (ECMWF) and observational case studies, *Teitelbaum and Sadourny* [1998] argued that planetary waves may be more important than orographic gravity waves in determining the presence of PSCs under appropriate background temperature conditions. Ground based lidar measurements at Davis, Antarctica (69° S, 78°E), a location far from large mountain ranges, showed that planetary wave temperature perturbations were significantly more important than gravity wave perturbations in determining the occurrence of PSCs [*Innis and Klekociuk*, 2006]. PSCs can also be formed by inertia-gravity waves associated with upper tropospheric jet readjustment, as illustrated in a case study using lidar data from Syowa (69°S, 40°E) by *Shibata et al.* [2003]. Inertia-gravity waves originating from breaking Rossby waves on the polar jet front were identified as the source of some PSCs in the Arctic [*Hitchman et al.*, 2003].

[5] Many in situ and satellite observations have characterized orographic gravity wave activity in the stratosphere above the Antarctic Peninsula, either as monthly or seasonal averages of temperature variance or potential energy [*Wu and Jiang*, 2002; *Baumgaertner and McDonald*, 2007; *Hei et al.*, 2008], momentum flux [*Vincent et al.*, 2007; *Hertzog et al.*, 2008], or as individual case studies where wave parameters could be derived [*Alexander and Teitelbaum*, 2007; *Plougonven et al.*, 2008]. Recently, *Alexander et al.* [2009] used the Constellation Observing System for Meteorology, Ionosphere and Climate (COSMIC) Global Positioning System Radio Occultation (GPS-RO) constellation to study changes in stratospheric gravity wave activity throughout the 2007 winter with 5 day temporal resolution and attributed the large, intermittent increases in temperature variance above the Antarctic Peninsula to orographically generated gravity waves.

[6] Concurrently, the Antarctic Peninsula region is still a focus of research efforts to understand PSC distribution, composition and occurrence. Cloud-Aerosol Lidar and Infrared Pathfinder Satellite Observations (CALIPSO) data were used to construct seasonal characteristics of PSC class composition, with the peninsula region identified as having a large occurrence frequency [*Pitts et al.*, 2007]. A CALIPSO case study of H_2O ice PSCs with high optical depth combined with high-resolution model simulations showed the central role of orographic gravity waves in causing its formation [*Noel et al.*, 2009]. *McDonald et al.* [2009] used Polar Ozone and Aerosol Measurement (POAM) III aerosol extinction and Challenging Minisatellite Payload (CHAMP) temperature profiles to show that gravity waves play an important role in the formation of PSCs early in the season when temperatures hover around the NAT formation threshold temperature T_{NAT}. The POAM III instrument used solar occultations, thus the southernmost latitude sampled varied during the PSC season. Nevertheless, *McDonald et al.*

[2009] found that about 40% of PSC formation above the peninsula could be explained by increases in CHAMP-observed temperature perturbations (i.e., gravity waves) early in the season, while gravity waves contributed to about 15% of PSC observed later in the season and away from the peninsula.

[7] While these and other case studies using observations and models have shown the clear relationship between gravity waves and PSC occurrence, until recently it has not been possible to characterize and quantify this relationship throughout an entire PSC season over an extended region. With the launches of the CALIPSO satellite and the COSMIC satellite constellation in 2006, PSCs and mesoscale gravity waves may now be resolved on spatial and temporal scales that allow quantification of the effect of orographic waves on H_2O ice PSC formation and occurrence. We use the results from the first complete Antarctic winter of operation of both observation platforms, 2007, to show the distribution of different PSC composition classes and their relation to orographic gravity waves and planetary waves. We quantify the contribution of orographic gravity waves above the peninsula on PSC formation and consider its downstream effects in terms of the seeding of NAT mother clouds. Our results show that while planetary waves are the primary controller of the occurrence of PSCs in the Antarctic when $T \sim T_{NAT}$, gravity waves above the Antarctic Peninsula cause H_2O ice formation which lead to significant increases in NAT PSCs downstream. Over the whole season in the 60°S–70°S latitude band, these peninsula orographic waves account for about 50% of the total H_2O ice PSC spatial volume and 30% of the total PSC spatial volume around Antarctica.

2. Data Sets

2.1. CALIPSO

[8] The CALIPSO satellite was launched in 2006 and is part of NASA's A-train satellite constellation [*Winker et al.*, 2007]. On board CALIPSO is the nadir-viewing lidar Cloud-Aerosol Lidar with Orthogonal Polarization (CALIOP), which provides curtains of backscatter ratio from the surface to 40 km, except when blocked by very thick tropospheric cloud. CALIOP is ideally suited for the observation of PSCs because of its ability to observe these clouds irrespective of tropospheric weather conditions which often hamper ground-based measurements. We only consider CALIOP night passes as these have a higher signal-to-noise ratio, which allows detection of fainter PSCs. All results presented here use the v2.01 CALIOP Level 1B Profile data products. A PSC detection algorithm for CALIOP was developed by *Pitts et al.* [2007] before being extended by *Pitts et al.* [2009] in order to improve detection of tenuous PSCs, mainly of the NAT variety. This algorithm also discriminates the PSCs into four composition classes and is used in the present work. The full details of the algorithm are given by *Pitts et al.* [2009], but we summarize the key steps below.

[9] The 532 nm scattering ratio R_{532} and the 532 nm perpendicular backscattering coefficient β_{perp} are used to identify statistical outliers in the background stratospheric aerosol population as follows. First, the data are interpolated to 180 m vertical resolution. In order to extract all PSCs,
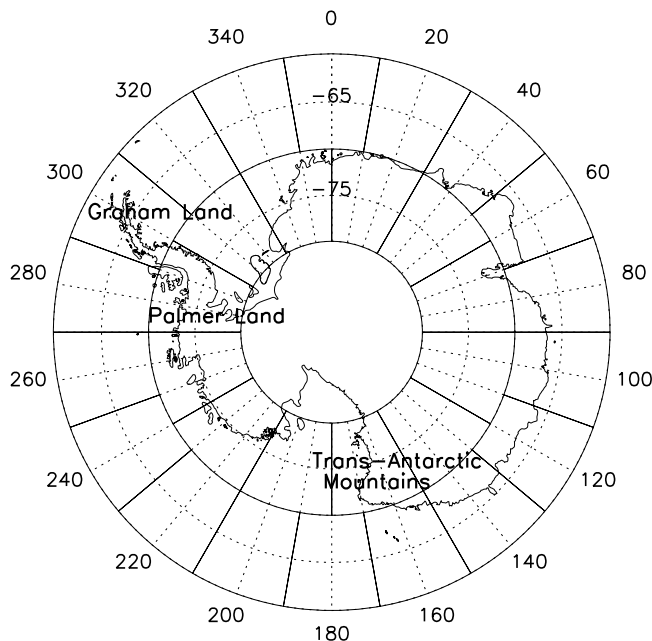
Figure 1. Spatial extent of grid cells used to bin the satellite data.

four passes are made through the data at increasingly coarse spatial resolutions of 5, 15, 45 and 135 km. At each horizontal resolution, profiles of R_{532} and β_{perp} are constructed, cloud detection thresholds applied, PSC occurrences flagged, and these data removed from subsequent processing and calculation of cloud thresholds at coarser resolution. The coarser horizontal resolutions are necessary to extract tenuous NAT and NAT-like clouds from the R_{532} and β_{perp}. Finally, all of the PSC-flagged data are collated at the end of the four passes. PSC detection thresholds are determined in 100 K thick potential temperature bands from 400 K to 700 K (overlapping by 50 K), with the background aerosol population characterized by the distribution above $T = 200$ K to avoid PSC contamination. Small amounts of PSCs occur below 400 K, however, we restrict the minimum isentrope of this PSC analysis to 400 K for several reasons: the 400 K surface remains above the lowermost stratosphere [*Holton et al.*, 1995]; 400 K is high enough to discount any effects from cirrus clouds; and the volume of PSC below this isentrope is comparatively small. We note that an analysis incorporating data as low as 350 K revealed similar PSC distributions to those detailed below (not shown). A spatial coherence test is then applied to minimize false positives. This removes essentially all false positives associated with noise spikes which are spatially isolated, while retaining cloud features (which extend vertically and horizontally over much larger scales) and also retaining cloud elements at cloud boundaries [*Pitts et al.*, 2009].

[10] PSCs are separated into four composition classes based on aerosol depolarization, $\delta_{aerosol}$, and inverse scattering ratio, $1/R_{532}$. The class boundaries are illustrated in Figure 7 of *Pitts et al.* [2009]. The supercooled ternary solution (STS) class refers to predominantly liquid droplet PSCs with low $\delta_{aerosol}$. There are two liquid/NAT mixture composition classes, with mix 1 (mix 2) having lower (higher) NAT number densities. Finally, there is the ice

class, although as noted by *Pitts et al.* [2009], this composition class likely contains PSCs which are an ice-STS mix except in the case of orographic wave clouds.

2.2. COSMIC GPS-RO

[11] The six COSMIC GPS-RO satellites were launched in April 2006 and provide around 2000 occultation events per day around the globe [*Anthes et al.*, 2008]. Profiles from the COSMIC Data Analysis and Archive Center (CDAAC) version 2.0 dry temperature data product are used, with the temperatures of each profile rebinned to 1 km vertical resolution [*Baumgaertner and McDonald*, 2007; *S. P. Alexander et al.*, 2008]. Note that GPS-RO measurements are insensitive to the presence of PSCs [*Kursinski et al.*, 1997].

[12] Following an examination of the CALIPSO and COSMIC data coverage, we bin the satellite results into grid cells with longitude width 20° and latitude width 10° centered on 65°S. Data centered on 75°S are also binned into cells with latitude width 10°, but due to the lower COSMIC data rates in this latitude range, encompass 30° in longitude. The grid cells are shown in Figure 1. The grid cells centered on [300°E, 65°S] and [285°E, 75°S] are collectively referred to as the Antarctic Peninsula. The northern grid cell contains Graham Land, while the southern cell covers Palmer Land and the Ellsworth Mountains. Temperature perturbations due to orographic gravity wave activity often extend well to the east (downwind) of the peninsula [*Wu and Jiang*, 2002; *Alexander and Teitelbaum*, 2007].

[13] The temporal resolution of these grid cells is 7 days, stepped forward in time by 1 day. This is lower than the 5 days used by *Alexander et al.* [2009], however it is necessary here to allow for sufficient CALIPSO spatial coverage. The lapse rate tropopause is calculated for each temperature profile, after which the stratospheric temperature component (defined as the altitudes between the tropopause and 25 km above the tropopause) is extracted. Its linear trend in altitude is removed via a linear least squares fit and the result is fitted to a cubic polynomial (different order polynomials return nearly identical results, not shown). This analysis method avoids residual effects which would result from the tropopause temperature gradient [*de la Torre et al.*, 2006; *Schmidt et al.*, 2008]. The resulting perturbations $T'(z)$ are then zero padded and high-pass filtered with the cutoff at 15 km. The temperature variance σ^2 calculated for each profile from these filtered perturbations is attributed to gravity wave activity. The variances from each perturbation profile are combined into a 7 day grid cell average. While this method does not actively remove planetary waves, the perturbation effects due to gravity waves are generally much larger than those due to planetary waves [see *McDonald et al.*, 2010, Figure 4].

[14] As with any observational technique, only a limited part of the gravity wave spectrum is resolvable with COSMIC. In this case, we can consider waves with vertical wavelengths λ_z between ~2 km and 15 km. GPS-RO is sensitive to waves which have horizontal wavelengths $\lambda_x >$ 150 km when the wavefronts are perpendicular to the line of sight (LOS) of the occultation with temperature perturbations from shorter λ_x waves being smeared out [*de la Torre and Alexander*, 2005; *P. Alexander et al.*, 2008; *McDonald and Hertzog*, 2008]. The resolution is about an order of

magnitude better when wavefronts are parallel to the LOS [*Kursinski et al.*, 1997]. *Alexander et al.* [2009] analyzed the COSMIC LOS during austral winter 2007 and found a bias toward the north-south axis, resulting in an increased likelihood of orographic wave detection above the peninsula. Mountain waves are also highly intermittent, with individual waves only persisting for a few hours [*Noel et al.*, 2009]. However, given that orographic waves seen in the stratosphere are generated by tropospheric synoptic conditions (e.g., eastward surface winds over a mountain range, with low wind rotation angle in the troposphere) which may persist for several days [*Fueglistaler et al.*, 2003], while individual wave parameters are generally irresolvable, the overall increased σ^2 is still observable. Nevertheless, short bursts of intense wave activity seen in some individual profiles [*Baumgaertner and McDonald*, 2007] will be missed in this 7 day running mean analysis. Some peninsula mountain waves have $\lambda_z > 15$ km and $\lambda_x < 150$ km in the stratosphere [*Alexander and Teitelbaum*, 2007; *Plougonven et al.*, 2008]. Stronger winds enhance wave activity by Doppler-shifting waves to longer λ_z. This may result in some waves being refracted outside the ~2 km < λ_z < 15 km observational filter window [*Alexander*, 1998]. Given the GPS-RO observational filtering and the high-pass filtering of the data, it is likely that COSMIC does not capture all of the orographic waves generated. GPS-RO is more likely to observe waves with short λ_z which have slow vertical group velocities c_{gz} due to their longer dwell time (compare this with Microwave Limb Sounder (MLS) which observes very long λ_z and fast c_{gz} [*Wu and Waters*, 1996]). However, the close relationship between orographic gravity wave activity and H_2O ice PSCs to be shown below indicates that the slower gravity waves with $\lambda_z < 15$ km captured by this GPS-RO analysis correspond to the presence of the ice PSCs.

[15] In this analysis, we only use data between 60°S and 80°S. The CALIPSO satellite records data as far south as 82°S, however beyond 80°S the frequency of COSMIC occultations decreases significantly, thus not allowing the study of gravity waves on short enough time scales in the grid cells used here. The total PSC spatial volumes and percentage effects of orographic gravity waves discussed in this study therefore only refer to the latitudes between 60°S and 80°S. We will present the results in two separate latitude bands (60°S–70°S and 70°S–80°S) to emphasize the differences in PSC volumes as a result of the former latitude band being warmer and closer to (and occasionally outside) the vortex edge.

2.3. MLS

[16] The Earth Observing System (EOS) Microwave Limb Sounder (MLS) flies onboard the Aura satellite, which was launched in July 2004. MLS collects information on a wide variety of atmospheric chemical species and also provides temperature and geopotential height data equatorward of 82° [*Waters et al.*, 2006]. Of relevance to the present study are the validated concurrent version 2.2 measurements of HNO_3 [*Santee et al.*, 2007], H_2O [*Lambert et al.*, 2007] and T [*Schwartz et al.*, 2008] in the stratosphere. A cold bias of around 2 K was observed in the MLS temperature data in the lower stratosphere [*Schwartz et al.*, 2008]. Despite this bias and despite MLS having lower resolution than operational reanalyses, we use MLS temperature data here

because it provides consistency with the trace gas species data. For H_2O, the estimated precision is 0.2–0.5 ppmv (4%–11%) in the pressure range 68–0.01 hPa [*Lambert et al.*, 2007], while the HNO_3 measurements are uniformly biased low by 10%–30% throughout most of the stratosphere [*Santee et al.*, 2007]. The NAT and H_2O ice temperature formation thresholds are calculated from these data (referred to as T_{NAT} and T_{ice}, respectively), following *Hanson and Mauersberger* [1988] and *Marti and Mauersberger* [1993]. In calculating these formation thresholds, we have not adjusted for biases in the MLS measurements other than following the standard quality control guidelines of *Santee et al.* [2007] and *Schwartz et al.* [2008]. The water vapor vertical artefact in MLS measurements between 31.6–26.1 hPa noted by *Lambert et al.* [2007] is above the height range of interest for our study. The data are binned into the same grid cells as used for COSMIC and CALIPSO. MLS data are obtained on a daily basis, therefore the results illustrated below are 7 day boxcar averaged to match the temporal resolution of COSMIC and CALIPSO, with data gaps linearly interpolated.

3. PSC Location and Occurrence

3.1. Background Conditions

[17] Hövmoller diagrams of the COSMIC temperature and σ^2 are shown throughout winter 2007 on the 550 K isentrope in Figure 2. We choose 550 K (~22–23 km altitude) as this is close to the coldest altitude; it is the central isentropic surface in the 400–700 K PSC analysis range; and it is also where gravity wave amplitudes are sufficiently large to be clearly resolvable above the background. Large amounts of planetary wave activity with zonal wave numbers 1 and 2 are seen in the temperature data, which are either eastward propagating or quasi-stationary (a detailed analysis of these planetary waves is provided by *Alexander and Shepherd* [2010]). The coldest longitudinal regions at 60°S–70°S are over the 270°E–0°E sector during August and September. Large, intermittent σ^2 is observed above the peninsula throughout winter.

[18] The 7 day smoothed COSMIC temperatures and COSMIC-derived gravity wave variances σ^2 during winter 2007 are shown for the grid cell centered on the northern half of the peninsula at [300°E, 65°S] in Figure 3. Increases in σ^2 occur throughout winter and only during times when there is no United Kingdom Meteorological Office (UKMO) assimilated [*Swinbank and O'Neill*, 1994] tropospheric 0 m s^{-1} zonal wind line (not shown), as this inhibits propagation of orographic gravity waves. *Alexander et al.* [2009] reported that all of these regions of large gravity wave activity during this winter are likely due to orographic waves, given the low wind rotation angles and lack of a 0 m s^{-1} line. The H_2O ice PSC area from CALIPSO is also marked in Figure 3. The relation between ice PSC occurrence and large σ^2 is readily apparent throughout winter and will be investigated fully below. Large cirrus cloud decks are visible at 10–12 km, often below regions of H_2O ice PSC.

3.2. 2007 Winter PSC Composition Class Distribution

[19] CALIPSO has the unique capability of providing observational estimates of PSC spatial volumes [*Pitts et al.*, 2009]. The total winter (1 June to 1 October) volumes of
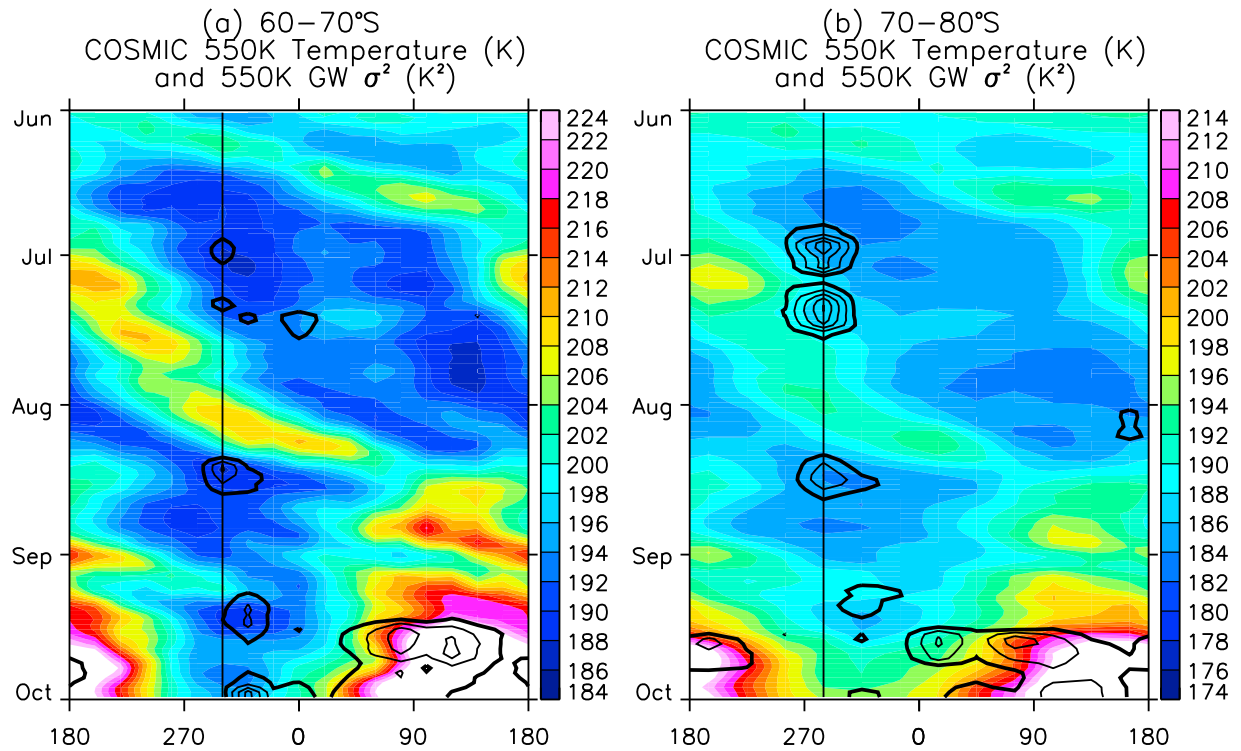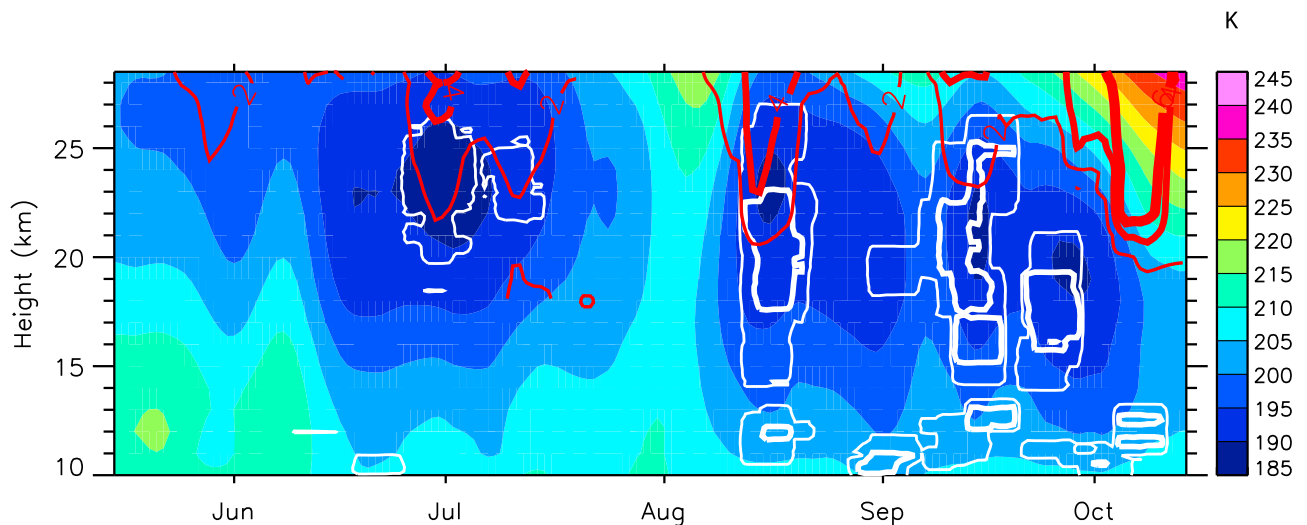
Figure 2. COSMIC temperatures (color contours) and σ^2 (black lines, units of K^2, interval 1 K^2, first (thick) contour at 2 K^2) on the 550 K isentrope: (a) 60°S–70°S (the vertical line indicates the longitude of Graham Land) and (b) 70°S–80°S (the vertical line indicates the longitude of Palmer Land). Note the different temperature scales. White data exceed the maximum contour level. The y axis tick marks indicate the start of each month.

PSCs at 400–700 K from each composition class are shown as a function of longitude at 60°S–70°S in Figure 4a and at 70°S–80°S in Figure 4b.

[20] The peak H_2O ice volume at 60°S–70°S corresponds to the largest σ^2 above the Antarctic Peninsula, with a minimum around 220°E (Figure 4a). A secondary increase in σ^2 and H_2O ice volume is visible along the coastline of Eastern Antarctica, although some of this σ^2 is related to the decaying vortex from mid-September onward (discussed below). While the peak H_2O ice volume occurs at 300°E,

Figure 3. COSMIC temperatures (color, units of K) and COSMIC σ^2 (red lines, units of K^2, first contour at 2 K^2, contour interval 2 K^2) above Graham Land during winter 2007. The H_2O ice PSC area contours at 0.02 million km^2 (0.1 million km^2) are marked by the thin (thick) white lines. The x axis tick marks indicate the start of each month.
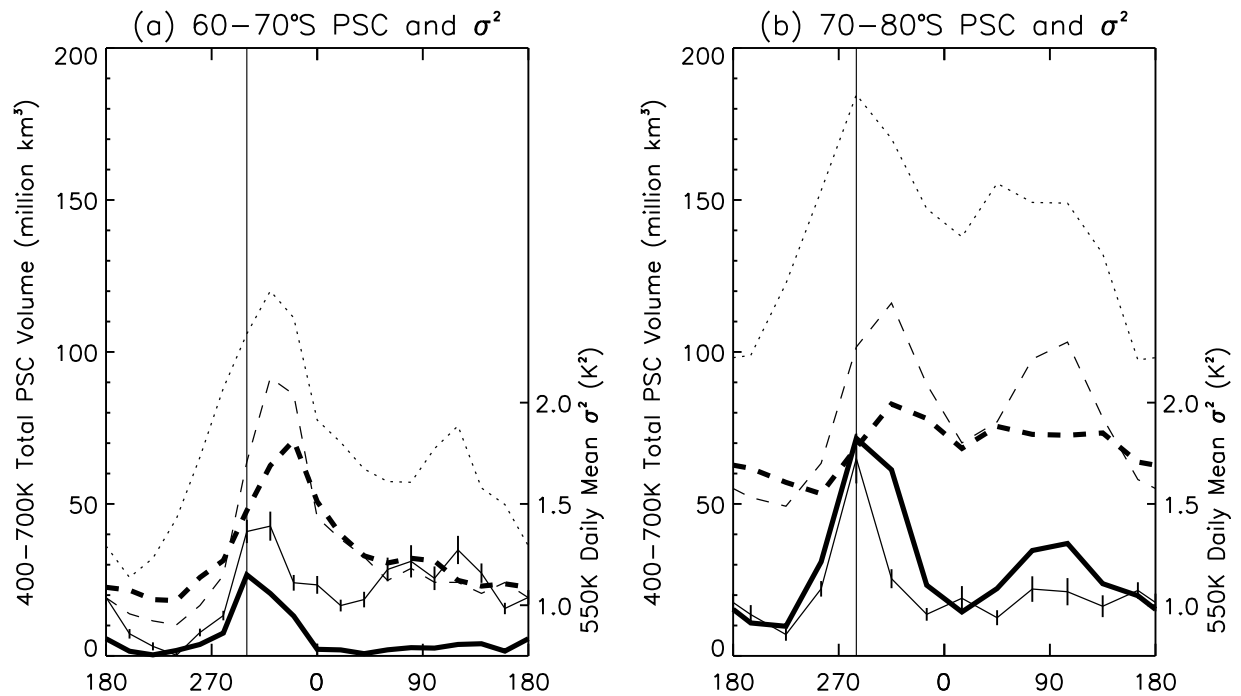
Figure 4. Total winter (1 June to 1 October) PSC volumes at 400–700 K for the various composition classes at (a) 60°S–70°S (the vertical line indicates the longitude of Graham Land) and (b) 70°S–80°S (the vertical line indicates the longitude of Palmer Land). The composition classes, with scale to the left, are marked as follows: ice (thick solid), mix 1 (thick dashed), mix 2 (thin dashed), and STS (thin dotted). The 550 K daily mean σ^2 is also marked (thin solid, scale to the right; uncertainty bars indicate the standard errors). The x axis tick marks indicate longitude east.

the peaks of mix 1, mix 2 and the STS volumes occur downwind of the peninsula, either at 320°E (mix 2 and STS) or 340°E (mix 1). These seasonal observations lend initial support to the mountain wave seeding hypothesis of PSCs, where a relatively small temperature perturbation influences the PSC occurrence at considerable distances downwind in the NAT freezing belt [*Höpfner et al.*, 2006]. The total winter H_2O ice volume above Graham Land (300°E) is 26 million km^3, which is about three times that at 280°E (8 million km^3) and more than six times that at 260°E (4 million km^3). Downwind of Graham Land, the H_2O ice volumes remain elevated: 21 million km^3 at 320°E and 13 million km^3 at 340°E. Note the large longitudinal extent over which the mix 1 and mix 2 NAT PSC classes remain enhanced downwind of the peninsula.

[21] The largest winter total H_2O ice volume at 70°S–80°S once again is located above the peninsula, at the same longitude as the largest daily mean σ^2 (Figure 4b). Most of the large σ^2 around 90°E is related to the decaying vortex in spring and not to orographic wave activity. A secondary peak in H_2O ice volume occurs above the East Antarctic plateau. Peak STS is recorded above the peninsula, while peak mix 1 and mix 2 are at 315°E, immediately downwind of the peninsula. The total winter H_2O ice volume above Palmer Land (285°E) is 72 million km^3, which is over double that at 255°E (31 million km^3) but similar to that at 315°E (61 million km^3). The total winter H_2O ice volume above Palmer Land is around three times that above Graham Land. Part of the reason for the similar H_2O ice volume directly downwind of Palmer Land is the geographical

extent of the grid cells: the cell centered on 315°E is close to the coastline and likely has large amounts of H_2O ice advected into its western edge (Figure 1).

[22] The results presented in Figure 4 strongly suggest the important role that orographic gravity waves play in forming H_2O ice PSCs that then seed significant amounts of NAT formation downstream. Before we quantify the contribution of orographic waves to the total amount of PSCs observed, we will consider the varying background temperature due to the vortex and planetary waves. We will also isolate the orographic wave events to examine their characteristics in detail.

3.3. PSC Hövmoller Diagrams

[23] The relationship between MLS-derived $T - T_{ice}$ and H_2O ice PSCs, as well as the relationship between MLS-derived $T - T_{NAT}$ and the mixed class PSC occurrence is clearly illustrated in Hövmoller diagrams (Figures 5 and 6). In the 60°S–70°S latitude band (Figure 5), temperatures hover around T_{NAT} and thus require the presence of planetary waves to induce widespread adiabatic cooling for PSC formation [*Teitelbaum and Sadourny*, 1998]. Note that these planetary waves have periods of around 8–24 days [*Alexander and Shepherd*, 2010] and therefore monthly averaged stereographic plots of the distribution of PSCs around Antarctica will not capture the eastward movement of PSCs tied to planetary wave motion, likely missing the explanation of their occurrence. In Figure 5, regions where no STS or liquid/NAT mixed PSCs are present, such as from 180°E–270°E during July, are located outside the vortex.
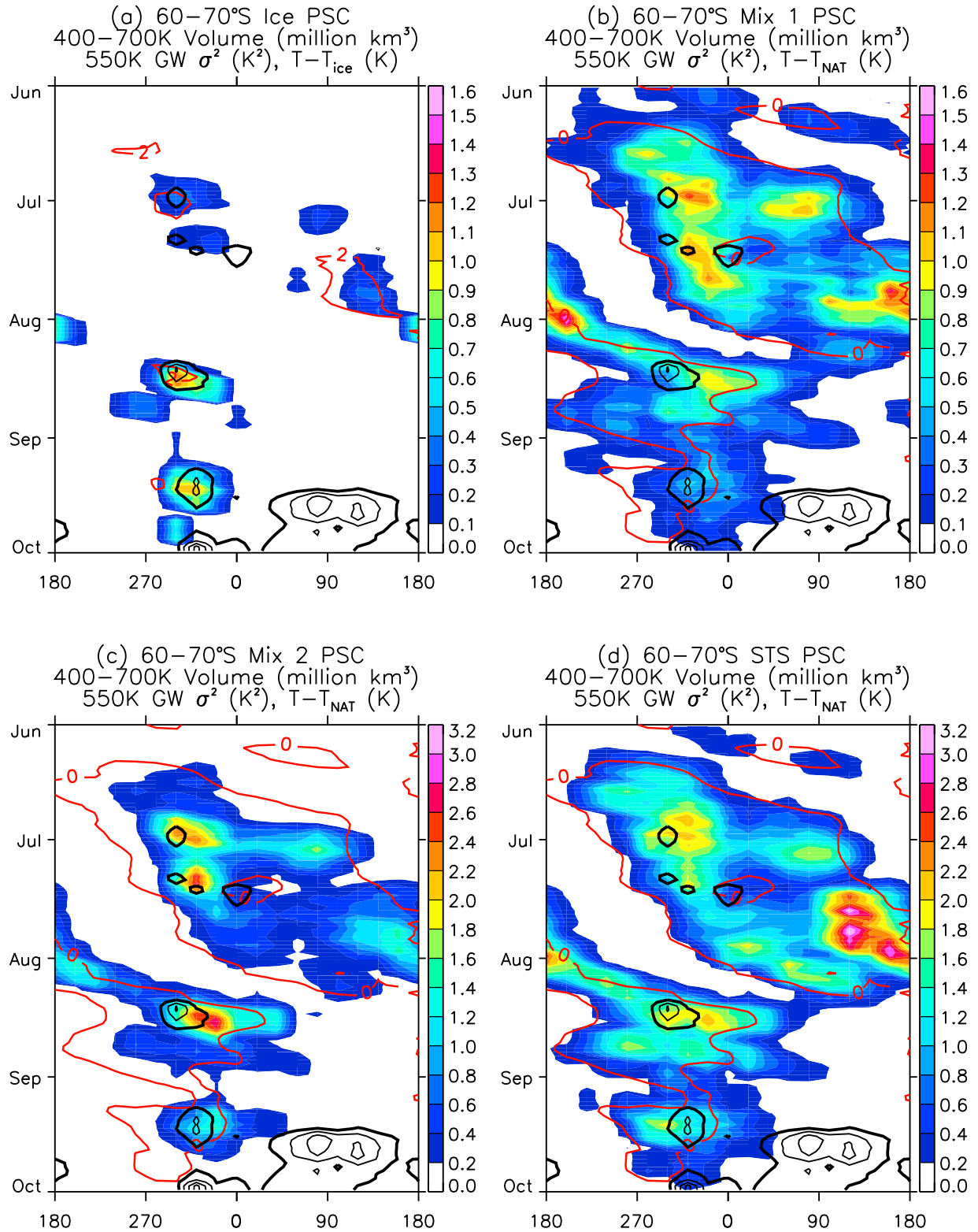
Figure 5. Hövmoller diagrams of PSC volume at 400–700 K and 60°S–70°S: (a) ice PSC, (b) mix 1 PSC, (c) mix 2 PSC, and (d) STS PSC. In each plot, the color scale is the volume (million km^3) and the black lines show the gravity wave σ^2 on the 550 K isentrope (units of K^2, interval 1 K^2, first (thick) contour at 2 K^2). The red lines mark $T - T_{ice}$ (contours at 0 K and 2 K) or $T - T_{NAT}$ (contour at 0 K) on the 550 K isentrope as indicated at the top of each plot. The y axis tick marks indicate the start of each month, and x axis tick marks indicate longitude east. Note that the PSC volume color scales for Figures 5a and 5b are half that of Figures 5c and 5d.
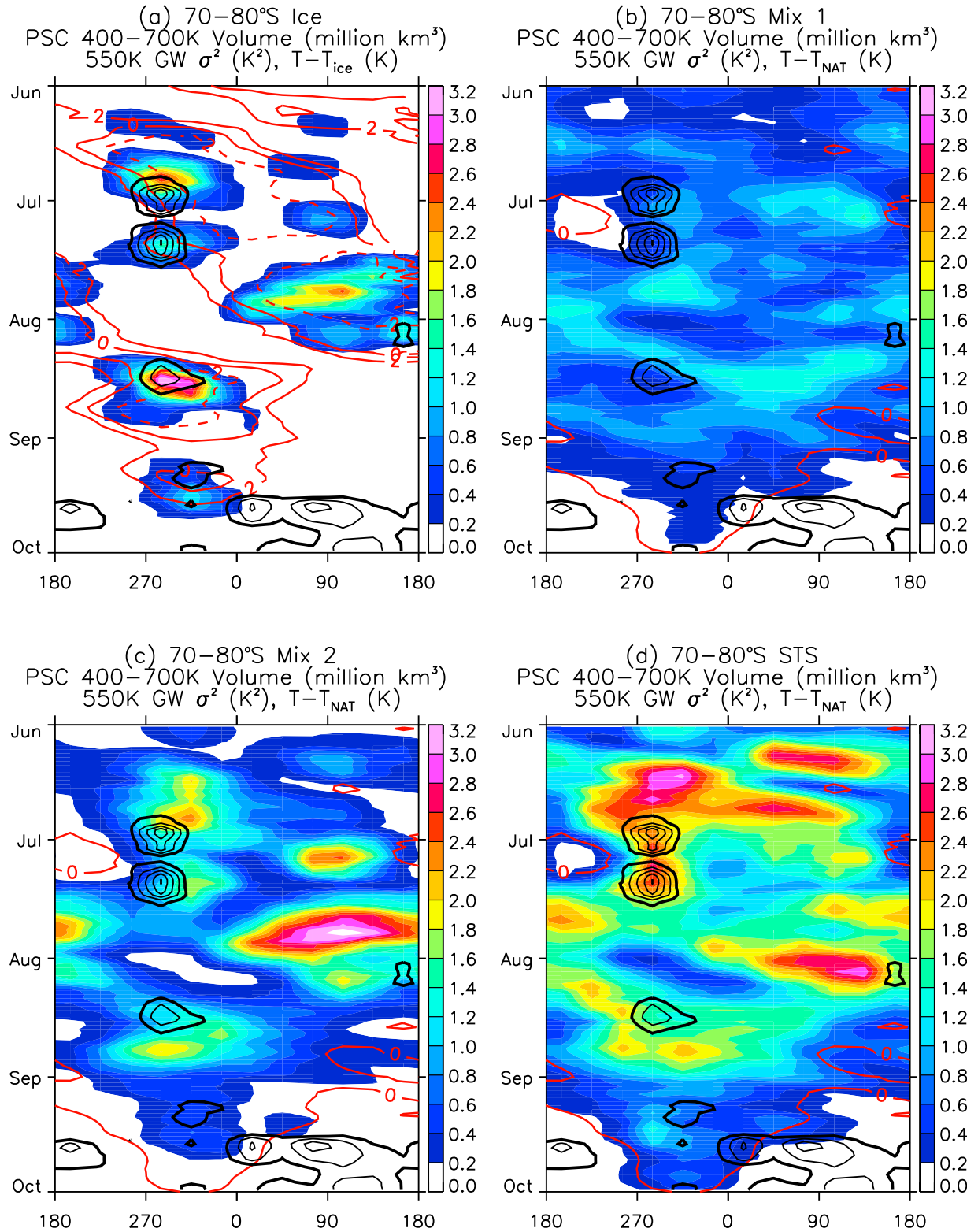
Figure 6. Same as Figure 5 but at 70°S–80°S. All volume color scales are the same. The $T - T_{ice}$ contours are plotted at −2 K (dashed), 0 K, and 2 K.

[24] There are several cases in Figure 5a where a close association between enhanced temperature variance and water ice PSCs exist above the peninsula region. During these times, we calculate the 550 K MLS $T - T_{ice}$ as being between 0 K and 2 K, although this difference may be up to ~1 K higher than shown on the basis of the biases noted in section 2.3. Figure 5a suggests that the H_2O ice PSCs associated with increased gravity wave temperature variance

are generally transported downwind by the background eastward flow, with significant volumes of ice visible later in time around to 0°E. The mountain wave regions are also associated with enhanced mix 2 PSCs (which have high NAT content), as seen in Figure 5c by the increased volumes downwind of Graham Land (longitude 300°E). The effects on mix 1 and STS PSC classes are smaller, although there are some clear cases such as the mid-August event where enhancements in both of these classes occur downstream from large orographic wave activity.

[25] The stratosphere at 70°S–80°S is colder, with a larger presence of all types of NAT and STS composition class PSCs (Figure 6) due to temperatures below T_{NAT} for nearly the entire winter at all longitudes. Large regions where temperatures are close to T_{ice} are also observed. The $T - T_{ice}$ field is not fully coincident with the H_2O ice PSC volume because the fairly coarse MLS spatial resolution does not fully capture mesoscale orographic gravity wave activity. (The along-track horizontal resolution of MLS is ~170 km, the across track resolution is ~12 km and the vertical resolution is around 4 km at PSC altitudes [*Schwartz et al.*, 2008].) MLS only observes mean temperature conditions, while the clouds are affected by the true local temperatures. MLS water vapor biases may also account for some of the discrepancies, but would only be important during the dehydrated period late in the PSC season (MLS H_2O measurements are unreliable below 0.1 ppmv). Sometimes the background temperature is cold enough for H_2O ice PSC formation in regions of low or no σ^2, especially above the East Antarctic plateau from mid-July until mid-August. Nevertheless, orographic wave activity above Palmer Land is still responsible for forming a significant amount of the observed H_2O ice PSCs. The H_2O ice PSCs begin to form above Palmer Land in late June [*Cariolle et al.*, 1989] prior to large wave activity, at a time when $T - T_{ice} \sim 0$ K for over a week. Enhancements in mix 2 PSC volume are seen throughout winter, mostly coincident with increased volumes of H_2O ice PSCs. In this higher-latitude band, the background temperatures remain below T_{NAT} for extended periods of time, allowing mix 2 PSCs which may have been nucleated downstream of orographic wave activity to persist for many days and advect around the vortex. This may explain the weaker relationship between peninsula gravity wave activity and mix 2 PSC volume.

[26] A small increase in σ^2 and H_2O ice PSC occurs in both latitude bands at the start of August around 180°E, which is a result of orographic wave activity from the Trans-Antarctic mountains [*Baumgaertner and McDonald*, 2007; *Noel et al.*, 2008; *Alexander et al.*, 2009].

4. PSCs in the Antarctic Peninsula Region

4.1. Orographic Gravity Waves and H_2O Ice PSCs

[27] The Hövmoller diagrams (Figures 5 and 6) illustrated that orographic gravity waves above the peninsula are generally necessary for the formation of H_2O ice PSCs at 60°S–70°S, while further south these waves increase the volume of H_2O ice PSC observed. We now investigate the relationship between $T - T_{ice}$, σ^2 and H_2O ice PSC in detail in Figure 7. For both latitude bands, we consider the results above the peninsula, directly upwind, directly downwind, and for comparison we also examine an average of East

Antarctic values across several grid cells. While we discuss T_{ice} and T_{NAT} values from MLS, these values are affected by uptake of HNO_3 onto clouds, leaving a reduced gas phase concentration measurable by MLS. This results in lower measured trace gas concentrations, resulting in lower T_{ice} and T_{NAT} values. However, even with a worst case scenario of a 30% low bias for HNO_3 [*Santee et al.*, 2007], the error in T_{NAT} is less than ~1 K at PSC formation altitudes. Note that T_{NAT} is more sensitive to variations in H_2O than it is to variations in HNO_3 [see, e.g., *McDonald et al.*, 2009, Figure 2].

[28] Results at 60°S–70°S are shown in Figure 7 (left). Generally, $T - T_{ice} > 0$ K, except briefly in mid-August and again in mid-September. The presence of orographic waves above Graham Land results in σ^2 increasing by 2–4 times that above the ocean, which is sufficient to cool the local atmosphere for the formation of large volumes of H_2O ice PSC. Despite the lower σ^2 at 320°E, significant amounts of H_2O ice PSC are still observed, which is likely a combination of the advection of PSCs formed to the west (as illustrated in Figure 5), and possible PSC formation occurring in orographic waves above this grid cell which extend from the mountains eastward. Above coastal East Antarctica, temperatures are coldest during the second half of July (Figure 2), during which time no increase in gravity wave activity is noted. However, the duration of this cold spell above coastal East Antarctica is clearly long enough to allow some H_2O ice PSC formation, although the volume formed is still at low levels when compared with that above Graham Land.

[29] The much colder atmosphere at 70°S–80°S is evident in the right hand column of Figure 7, where $T - T_{ice}$ drops to around −4 K. Several large increases in σ^2 occur above Palmer Land during the winter and all except the one in late May are associated with large amounts of H_2O ice PSC formation (as it was too warm in late May for H_2O ice PSC formation despite the presence of gravity waves). Low σ^2 but high ice PSC volume is observed downwind of Palmer Land. Immediately upwind (255°E), there are still reasonably large amounts of H_2O ice PSC. This is related to increases in σ^2 (this grid cell covers part of West Antarctica and some mountain ranges), with smaller amounts due to very cold conditions with little gravity wave activity, such as mid-June. Above the East Antarctic plateau, very cold conditions occur for four weeks from mid-July until mid-August and allow the formation of significant volumes of H_2O ice PSC.

4.2. Downstream Effects of Orographic Waves on NAT PSCs

[30] Buried inside the 60°S–70°S planetary wave related distributions of the mix 1, mix 2 and STS classes (Figure 5) are increases in their volumes coincident in time with the formation of H_2O ice by orographic waves. We investigate these changes in each composition class at 60°S–70°S in Figure 8. In each of the grid cells considered here, the $T - T_{NAT}$ are also displayed (Figure 8f). This quantity is negative for significant periods of time, mostly as a result of planetary wave activity. During late May and early June, when orographic wave activity was identified (Figure 7b), $T - T_{NAT} < 0$ briefly, which is long enough for a significant increase in the mix 1 PSC volume (Figure 8a). This early season orographic forcing results in an approximate dou-
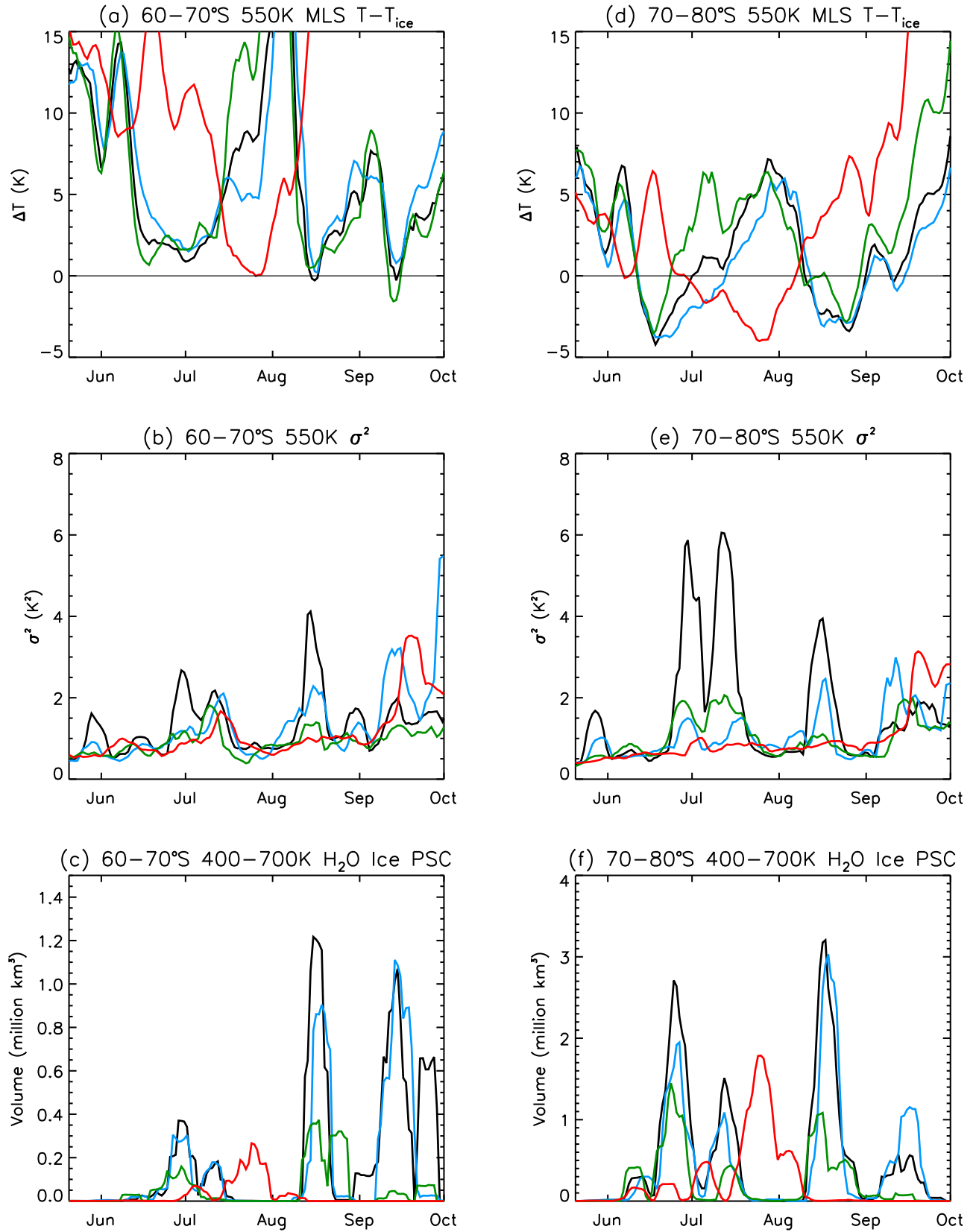
Figure 7. Comparisons of (a, d) MLS $T - T_{ice}$, (b, e) σ^2, and (c, f) H_2O ice PSC volume at 60°S–70°S and 70°S–80°S. For Figures 7a–7c, the grid cells are 280°E (green), 300°E (peninsula, black), 320°E (blue), and the average of 100°E–140°E (East Antarctic coastline, red). For Figures 7d–7f, the grid cells are 255°E (green), 285°E (peninsula, black), 315°E (blue), and the average of 45°E–135°E (East Antarctic plateau, red). Note the different H_2O ice PSC volume y axis scales for each latitude band.
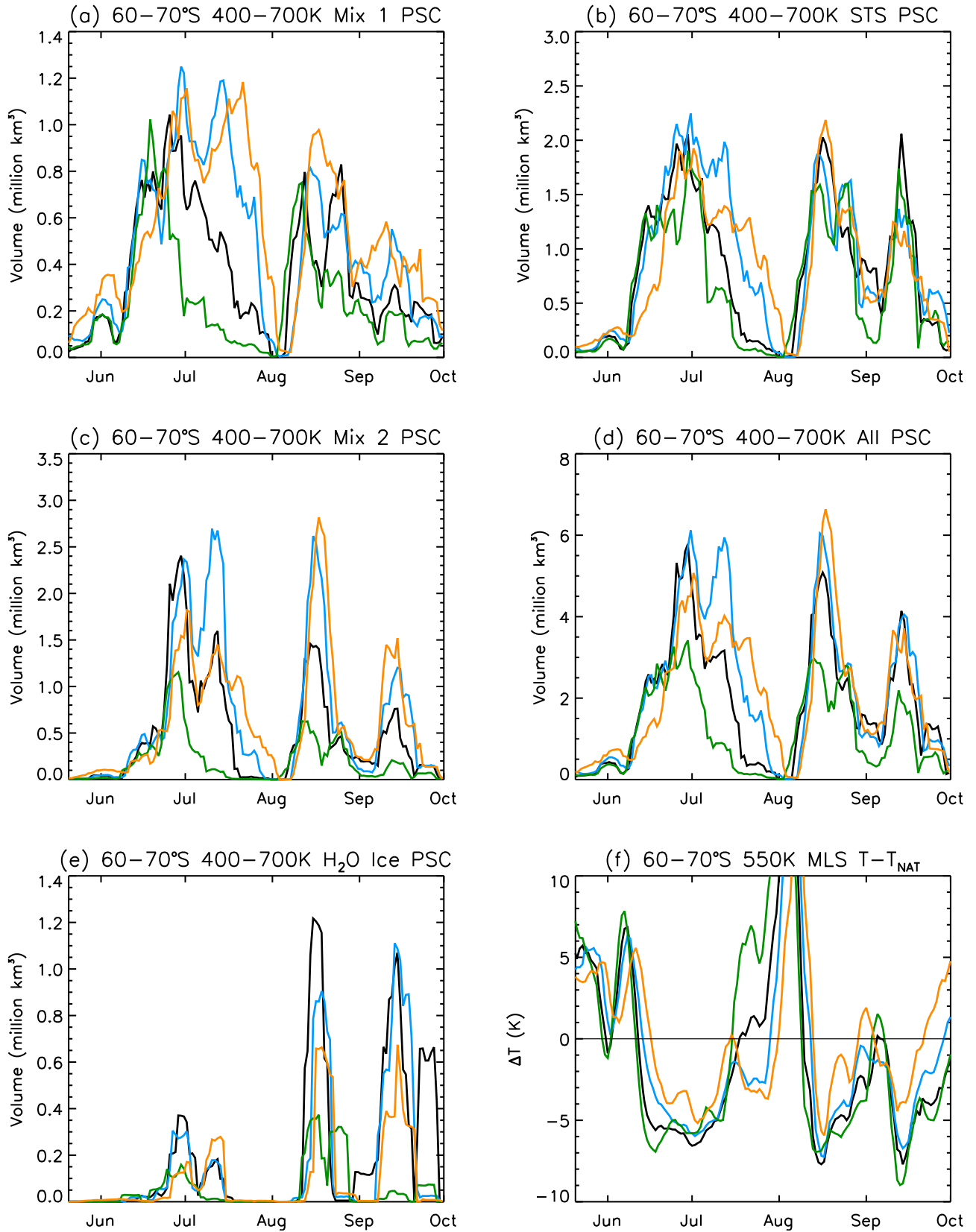
Figure 8. Time series at 60°S–70°S showing the PSC volume at 400–700 K of various PSC composition classes in grid cells: upwind of the peninsula (280°E, green), above the peninsula (300°E, black), and two cells downwind of the peninsula (320°E, blue and 340°E, orange). (a) Mix 1, (b) STS, (c) mix 2, (d) all PSC classes, and (e) H$_2$O ice PSCs. The y axis scales vary between plots. (e) The MLS $T - T_{NAT}$ with the colors as per Figures 8a–8d.

Table 1. The 2007 Winter (1 June to 1 October) Percentage of PSC Volume Attributed to Orographic Gravity Wave Activity Above the Antarctic Peninsula[a]

Latitude Band	PSC Composition Class	Attributed to Orographic Gravity Waves (%)
60°S–70°S	H_2O ice	50
60°S–70°S	liquid/NAT mix 1	30
60°S–70°S	liquid/NAT mix 2	50
60°S–70°S	STS	10
60°S–70°S	total	30
70°S–80°S	H_2O ice	20
60°S–80°S	H_2O ice	30

[a]Values are given to one significant figure. Uncertainties are on the order of 5%–10%.

bling of the mix 1 PSC volume above Graham Land and downstream. The H_2O ice PSC volume distributions in Figure 8e are the same as in Figure 7c, except with the replacement of the East Antarctic results by the grid cell at 340°E further downwind of Graham Land. The steady decrease in H_2O ice volume east of Graham Land is clearly apparent for all events except the small mid-July case. This is reversed for mix 1 and mix 2; that is, the volumes of these PSCs increase the further downwind one travels. These results are a clear indication of mountain wave seeding throughout the entire season, where the H_2O ice allows NAT mother clouds to form and subsequently to be advected downstream. While there are significant amounts of mix 1 and mix 2 upwind of Graham Land, these PSC composition classes still increase in volume downwind of the peninsula at and shortly after the time of large orographic gravity wave activity.

[31] There is little effect on STS volume in the presence of orographic gravity waves. STS is almost entirely related to the presence of planetary waves which provide cold enough conditions for their formation. For completeness the total PSC volume is also shown in Figure 8d. The total PSC volume is clearly enhanced above and downwind of the peninsula, although without the above separation into separate PSC composition classes, it is difficult to determine the contribution to total PSC volume from orographic wave forcing. The near-complete lack of PSCs in early August is because these grid cells were outside the vortex.

4.3. Quantification of PSCs due to Antarctic Peninsula Orographic Waves

[32] The winter mean PSC and σ^2 distribution of Figure 4 suggested the important role of mesoscale orographic gravity waves in determining PSC occurrence and composition at 60°S–70°S throughout winter. The detailed analysis of periods of large wave activity in the Hövmoller diagrams and the downstream effects for individual events (Figures 5 and 8) confirmed this initial interpretation.

[33] We now return to the total winter (1 June to 1 October) PSC volumes distributed in longitude (see Figure 4). To quantify the amounts of each PSC composition class due to orographic gravity waves above the peninsula and downstream at 60°S–70°S, we average the volumes in the grid cells at 260°E–280°E (the upwind ocean) and subtract this from the volumes in the peninsula region. We attribute the average ice PSC volume above the oceanic cells as being

due to nonorographic wave sources. We only use data in these two cells because of the presence of stationary planetary waves; that is, incorporating data much further westward affects the background state of the atmosphere which changes significantly due to stationary planetary waves and to movement into and out of the vortex (Figure 5). The downstream region is defined as those grid cells having larger volumes of PSCs than the upwind ocean threshold value. This region generally extends from the peninsula around to about 0°E–30°E (Figure 4). We are confident that these slightly enhanced PSC volumes this far east are related to peninsula orographic waves, given the results of Figure 5. The results of these calculations are summarized in Table 1. Around 50% of total H_2O PSC volume is attributable to orographic gravity wave activity at 60°S–70°S. The liquid/NAT mix 2 class also has around 50% of its volume attributable to orographic gravity wave activity. Values are also given for the STS and mix 1 classes in Table 1, however there are occasions (for example in early July) when the increased mix 1 volume does not propagate downstream at the same velocity as the gravity wave enhancement or the background wind (Figure 5).

[34] Changing the background definition to only incorporate the grid cell immediately upstream (280°E) results in decreases of the ice and NAT mixed class values by around 5%. These decreases are expected given the slightly colder grid cell immediately upstream of the peninsula (Figure 2) and the slightly larger PSC volumes (Figure 4) but does not alter the conclusion that orographic gravity waves are responsible for significant amounts of PSCs in this latitude band. The uncertainties in the percentage of PSCs attributable to orographic gravity wave activity are of the order of 5%–10%.

[35] The Hövmoller diagrams at 70°S–80°S (Figure 6) showed large increases in H_2O ice PSC volume during the presence of orographic gravity waves. There is some evidence for increases in mix 2 NAT downstream of the peninsula, but only sometimes following increases in H_2O ice PSCs (e.g., early July). The colder synoptic conditions allow the persistence of mix 2 particles, some of which were likely nucleated following orographic wave activity but have been advected significantly around the vortex. There is little if any enhancement observed in mix 1 or STS downstream of large H_2O ice PSC. Thus, the peaks observed in the total winter mix 1, mix 2 and STS volumes in Figure 4b downstream of the peninsula are mainly due to synoptic-scale conditions. We only calculate the H_2O ice PSC volume attributable to orographic gravity wave activity above the peninsula, which we determine to be 20%. Averaging the H_2O ice PSC volumes across the entire 60°S–80°S region results in around 30% being due to orographic gravity waves.

[36] An investigation using the annulus of data points between the vortex edge [Nash et al., 1996] and 10° inside the vortex edge was also conducted to attempt to trace PSC transport in a constant temperature region. The results from this annulus revealed a structure which combined features of Figures 5 and 6 (not shown), but due to a baroclinic environment, temperatures were not constant along the vortex edge [Mann et al., 2002]. This revealed that analyzing the data relative to the vortex edge provided no advantage to the

standard coordinate system because of the nonconstant dynamics.

5. Discussion

[37] The CALIPSO-COSMIC results indicate the important seasonal role of Antarctic Peninsula orographic gravity waves in providing local cooling for the formation of H_2O ice PSCs and subsequent NAT mother cloud seeding downstream in the NAT freezing belt [*Tabazadeh et al.*, 2001; *Dhaniyala et al.*, 2002; *Fueglistaler et al.*, 2002], despite the colder synoptic conditions inside the Antarctic polar vortex. These results confirm suggestions of *Höpfner et al.* [2006] and observations of *Eckermann et al.* [2009] and *McDonald et al.* [2009] that orographic wave triggered PSC formation is not unusual in the Antarctic and needs to be considered for the correct source attribution of the observed PSC distribution. The downstream effects on the liquid/NAT mixture PSCs indicate the same processes as those proposed by *Carslaw et al.* [1999] in the Arctic. Given the coincident increases in the two liquid/NAT mixture PSC composition classes downwind of the peninsula in the NAT freezing belt with orographic wave activity (Figures 4 and 8), the mechanism of orographic wave seeding of NAT mother clouds identified above Scandinavia [*Zondlo et al.*, 2000; *Fueglistaler et al.*, 2002; *Mann et al.*, 2005] clearly operates above the Antarctic Peninsula as well. While the Antarctic Peninsula is not the only region where orographic waves are generated (e.g., the Trans-Antarctic mountains are a secondary source of orographic wave activity [*Watanabe et al.*, 2006; *Baumgaertner and McDonald*, 2007]), during 2007 it was the location of nearly all resolvable orographic wave activity and subsequent PSC formation.

[38] Despite our results indicating the important role of orographic waves above the Peninsula in seeding NAT mother clouds, the dominant PSC formation condition in the Antarctic is the large-scale background temperature, which is modulated by planetary wave activity. The lower stratosphere is cold enough at 70°S–80°S for nearly continuous occurrence of NAT and STS PSCs regardless of planetary wave activity (Figure 6). However, at 60°S–70°S, temperatures are warmer and sufficiently close to T_{NAT} that NAT PSCs are only observed in the cold phases of the $s = 1$ and $s = 2$ planetary waves in the stratosphere, which is when this region is inside the vortex. *Teitelbaum and Sadourny* [1998] used ECMWF analyses to argue that PSC distribution can largely be explained by the adiabatic cooling of air within planetary wave structures. Using a lidar at Davis (69°S, 78°E), *Innis and Klekociuk* [2006] showed that planetary wave activity is the dominant factor controlling the occurrence of PSC above coastal East Antarctica. The relationship between PSC occurrence and planetary waves is observationally confirmed here for the entire winter around the latitude band where temperatures are close to T_{NAT} (Figure 5). These planetary waves have periods of less than one month [*Alexander and Shepherd*, 2010], thus it is important when considering the effects of planetary wave activity on PSCs around the edge of the vortex where $T \sim T_{NAT}$ that monthly averages of PSC occurrence distribution are not calculated otherwise correct attribution of their planetary and gravity wave formation origins becomes difficult.

[39] Antarctic gravity wave and planetary wave activities vary interanually [*Baumgaertner and McDonald*, 2007; *Hei et al.*, 2008; *Alexander and Shepherd*, 2010] which therefore affects the total PSC volume. The total PSC volume in the Antarctic vortex was lower during 2007 than during 2006 or 2008 due to a warmer 2007 vortex [*Pitts et al.*, 2009]. *Innis and Klekociuk* [2006] and *McDonald et al.* [2009] used ground- and space-based instruments, respectively, and even using different techniques they both reported that gravity waves affect PSC occurrence about 15% of the time except during early winter. Our results reveal similar values for the total PSCs due to orographic gravity waves (30% at 60°S–70°S, a value which would decrease if we could consider all latitudes poleward of 60°S). Given the demonstrated ability of CALIPSO and COSMIC to determine the relationship between PSCs and mesoscale gravity wave activity, it would be beneficial to extend these results across a multiyear time frame in both polar regions.

6. Conclusions

[40] The effect of orographic gravity waves on the occurrence and composition of PSCs was studied around Antarctica throughout the entire 2007 winter using CALIPSO and COSMIC data. Results were split into the two latitude bands of 60°S–70°S and 70°S–80°S, the former having synoptic-scale temperatures close to the PSC formation thresholds and being close to (or occasionally outside) the vortex edge.

[41] Results at 60°S–70°S showed the direct relation between orographic gravity waves above the Antarctic Peninsula and coincident H_2O ice PSC occurrence. These ice PSCs were then advected downstream, where enhancements in mixed liquid/NAT PSC composition classes occurred. The peak of H_2O ice PSC volume occurred above the peninsula, while the peak of the NAT classes occurred downstream. These results indicate the presence of mountain wave seeding throughout the Antarctic winter. In this latitude band, 30% of all PSCs during winter 2007 were attributed to peninsula orographic waves, while around 50% of both H_2O ice and mix 2 (high NAT number density) were due to these mountain waves.

[42] Due to the colder synoptic-scale temperatures at 70°S–80°S, the only PSC composition class for which an unequivocal volume increase related to orographic gravity waves was recorded was for the H_2O ice PSCs (20%). This resulted in a value of around 30% for the combined 60°S–80°S latitude bands. While we showed that planetary waves were the major determinant of PSC presence at temperatures close to the NAT formation threshold, we also demonstrated the important role of mesoscale, intermittent orographic gravity wave activity in accounting for the composition and distribution of PSCs around Antarctica.

References

Alexander, M. J. (1998), Interpretations of observed climatological patterns in stratospheric gravity wave variance, *J. Geophys. Res.*, *103*(D8), 8627–8640.

Alexander, M. J., and H. Teitelbaum (2007), Observation and analysis of a large amplitude mountain wave event over the Antarctic peninsula, *J. Geophys. Res.*, *112*, D21103, doi:10.1029/2006JD008368.

Alexander, P., A. de la Torre, and P. Llamedo (2008), Interpretation of gravity wave signatures in GPS radio occultations, *J. Geophys. Res.*, *113*, D16117, doi:10.1029/2007JD009390.

Alexander, S. P., and M. G. Shepherd (2010), Planetary wave activity in the polar lower stratosphere, *Atmos. Chem. Phys.*, *10*, 707–718.

Alexander, S. P., T. Tsuda, Y. Kawatani, and M. Takahashi (2008), Global distribution of atmospheric waves in the equatorial upper troposphere and lower stratosphere: COSMIC observations of wave mean flow interactions, *J. Geophys. Res.*, *113*, D24115, doi:10.1029/2008JD010039.

Alexander, S. P., A. R. Klekociuk, and T. Tsuda (2009), Gravity wave and orographic wave activity observed around the Antarctic and Arctic stratospheric vortices by the COSMIC GPS-RO satellite constellation, *J. Geophys. Res.*, *114*, D17103, doi:10.1029/2009JD011851.

Anthes, R. A., et al. (2008), The COSMIC/FORMOSAT-3 mission early results, *Bull. Am. Meteorol. Soc.*, *89*(3), 313–333, doi:10.1175/BAMS-89-3-313.

Baumgaertner, A. J. G., and A. J. McDonald (2007), A gravity wave climatology for Antarctic compiled from Challenging Minisatellite Payload Global Positioning System (CHAMP/GPS) radio occultations, *J. Geophys. Res.*, *112*, D05103, doi:10.1029/2006JD007504.

Cariolle, D., S. Muller, and F. Cayla (1989), Mountain waves, polar stratospheric clouds and the ozone depletion over Antarctica, *J. Geophys. Res.*, *94*(D9), 11,233–11,240.

Carslaw, K. S., et al. (1998a), Increased stratospheric ozone depletion due to mountain induced atmospheric waves, *Nature*, *391*, 675–678.

Carslaw, K. S., M. Wirth, A. Tsias, B. P. Luo, A. Dörnbrack, M. Leutbecher, H. Volkert, W. Renger, J. T. Bacmeister, and T. Peter (1998b), Particle microphysics and chemistry in remotely observed mountain polar stratospheric clouds, *J. Geophys. Res.*, *103*(D5), 5785–5796.

Carslaw, K. S., T. Peter, J. T. Bacmeister, and S. D. Eckermann (1999), Widespread solid particle formation by mountain waves in the Arctic stratosphere, *J. Geophys. Res.*, *104*(D1), 1827–1836.

de la Torre, A., and P. Alexander (2005), Gravity waves above Andes detected from GPS radio occultation temperature profiles: Mountain forcing?, *Geophys. Res. Lett.*, *32*, L17815, doi:10.1029/2005GL022959.

de la Torre, A., T. Schmidt, and J. Wickert (2006), A global analysis of wave potential energy in the lower stratosphere derived from 5 years of GPS radio occultation data with CHAMP, *Geophys. Res. Lett.*, *33*, L24809, doi:10.1029/2006GL027696.

Dhaniyala, S., K. A. Mckinnery, and P. O. Wennberg (2002), Lee-wave clouds and denitrification of the polar stratosphere, *Geophys. Res. Lett.*, *29*(9), 1322, doi:10.1029/2001GL013900.

Dörnbrack, A., T. Birner, A. Fix, H. Flentje, A. Meister, H. Schmid, E. V. Browell, and M. J. Mahoney (2002), Evidence for inertia gravity waves forming polar stratospheric clouds over Scandinavia, *J. Geophys. Res.*, *107*(D20), 8287, doi:10.1029/2001JD000452.

Drdla, K., M. R. Schoeberl, and E. V. Browell (2002), Microphysical modeling of the 1999–2000 Arctic winter: 1. Polar stratospheric clouds, denitrification, and dehydration, *J. Geophys. Res.*, *107*, 8312, doi:10.1029/2001JD000782 [printed *108*(D5), 2003].

Eckermann, S. D., L. Hoffmann, M. Höpfner, D. L. Wu, and M. J. Alexander (2009), Antarctic NAT PSC belt of June 2003: Observational validation of the mountain wave seeding hypothesis, *Geophys. Res. Lett.*, *36*, L02807, doi:10.1029/2008GL036629.

Fueglistaler, S., B. P. Luo, C. Voigt, K. S. Carslaw, and T. Peter (2002), NAT-rock formation by mother clouds: A microphysical model study, *Atmos. Chem. Phys.*, *2*, 93–98.

Fueglistaler, S., S. Buss, B. P. Luo, H. Flentje, C. A. Hostetler, L. R. Poole, K. S. Carslaw, and T. Peter (2003), Detailed modeling of moutain wave PSCs, *Atmos. Chem. Phys.*, *3*, 697–712.

Hanson, D., and K. Mauersberger (1988), Laboratory studies of the nitric acid trihydrate: Implications for the south polar stratosphere, *Geophys. Res. Lett.*, *15*, 855–858.

Hei, H., T. Tsuda, and T. Hiroka (2008), Characteristics of atmospheric gravity wave activity in the polar regions revealed by GPS radio occul-

tation data with CHAMP, *J. Geophys. Res.*, *113*, D04107, doi:10.1029/2007JD008938.

Hertzog, A., G. Boccara, R. A. Vincent, F. Vial, and P. Cocquerez (2008), Estimation of gravity wave momentum flux and phase speeds from quasi-Lagrangian stratospheric balloon flights. Part II: Results from the Vorcore campaign in Antarctica, *J. Atmos. Sci.*, *65*, 3056–3070.

Hitchman, M. H., M. L. Buker, G. J. Tripoli, E. V. Browell, W. B. Grant, T. J. McGee, and J. F. Burris (2003), Nonorographic generation of Arctic polar stratospheric clouds during December 1999, *J. Geophys. Res.*, *108*(D5), 8325, doi:10.1029/2001JD001034.

Holton, J. R., P. H. Haynes, M. E. McIntyre, A. R. Douglass, R. B. Rood, and L. Pfister (1995), Stratosphere-troposphere exchange, *Rev. Geophys.*, *33*(4), 403–439.

Höpfner, M., et al. (2006), MIPAS detects Antarctic stratospheric belt of NAT PSCs caused by mountain waves, *Atmos. Chem. Phys.*, *6*, 1221–1230.

Innis, J. L., and A. R. Klekociuk (2006), Planetary wave and gravity wave influence on the occurrence of polar stratospheric clouds over Davis Station, Antarctica, seen in lidar and radiosonde observations, *J. Geophys. Res.*, *111*, D22102, doi:10.1029/2006JD007629.

Kursinski, E. R., G. A. Hajj, J. T. Schofield, R. P. Linfield, and K. R. Hardy (1997), Observing Earth's atmosphere with radio occultation measurements using the Global Positioning System, *J. Geophys. Res.*, *102*(D19), 23,429–23,465.

Lambert, A., et al. (2007), Validation of the Aura Microwave Limb Sounder middle atmosphere water vapor and nitrous oxide measurements, *J. Geophys. Res.*, *112*, D24S36, doi:10.1029/2007JD008724.

Lowe, D., and A. R. MacKenzie (2008), Polar stratospheric cloud microphysics and chemistry, *J. Atmos. Sol. Terr. Phys.*, *70*, 13–40.

Mann, G. W., S. Davies, K. S. Carslaw, M. P. Chipperfield, and J. Kettleborough (2002), Polar vortex concentricity as a controlling factor in Arctic denitrification, *J. Geophys. Res.*, *107*(D22), 4663, doi:10.1029/2002JD002102.

Mann, G. W., K. S. Carslaw, M. P. Chipperfield, and S. Davies (2005), Large nitric acid trihydrate particles and denitrification caused by mountain waves in the Arctic stratosphere, *J. Geophys. Res.*, *110*, D08202, doi:10.1029/2004JD005271.

Marti, J., and K. Mauersberger (1993), A survey and new measurements of ice vapor pressure at temperatures between 170 and 250 K, *Geophys. Res. Lett.*, *20*, 363–366.

McDonald, A. J., and A. Hertzog (2008), Comparison of stratospheric measurements made by CHAMP radio occultation and Strateole/Vorcore in situ data, *Geophys. Res. Lett.*, L11805, doi:10.1029/2008GL033338.

McDonald, A. J., S. E. George, and R. M. Woollands (2009), Can gravity waves significantly impact PSC occurrence in the Antarctic?, *Atmos. Chem. Phys.*, *9*, 8825–8840.

McDonald, A. J., B. Tan, and X. Chu (2010), Role of gravity waves in the spatial and temporal variability of stratospheric temperature measured by COSMIC/FORMOSAT-3 and Rayleigh lidar observations, *J. Geophys. Res.*, *115*, D19128, doi:10.1029/2009JD013658.

Nash, E. R., P. A. Newman, J. E. Rosenfeld, and M. R. Schoeberl (1996), An objective determination of the polar vortex using Ertel's potential vorticity, *J. Geophys. Res.*, *101*(D5), 9471–9478.

Noel, V., A. Hertzog, H. Chepfer, and D. M. Winker (2008), Polar stratospheric clouds over Antarctica from the CALIPSO spaceborne lidar, *J. Geophys. Res.*, *113*, D02205, doi:10.1029/2007JD008616.

Noel, V., A. Hertzog, and H. Chepfer (2009), CALIPSO observations of wave-induced PSCs with near-unity optical depth over Antarctica in 2006–2007, *J. Geophys. Res.*, *114*, D05202, doi:10.1029/2008JD010604.

Pitts, M. C., L. W. Thomason, L. R. Poole, and D. M. Winker (2007), Characterization of polar stratospheric clouds with spaceborne lidar: CALIPSO and the 2006 Antarctic season, *Atmos. Chem. Phys.*, *7*, 5207–5228.

Pitts, M. C., L. R. Poole, and L. W. Thomason (2009), CALIPSO polar stratospheric cloud observations: second generation detection algorithm and composition discrimination, *Atmos. Chem. Phys.*, *9*, 7577–7589.

Plougonven, R., A. Hertzog, and H. Teitelbaum (2008), Observations and simulations of a large amplitude mountain wave breaking over the Antarctic Peninsula, *J. Geophys. Res.*, *113*, D16113, doi:10.1029/2007JD009739.

Santee, M. L., et al. (2007), Validation of the Aura Microwave Limb Sounder HNO$_3$ measurements, *J. Geophys. Res.*, *112*, D24S40, doi:10.1029/2007JD008721.

Schmidt, T., A. de la Torre, and J. Wickert (2008), Global gravity wave activity in the tropopause region from CHAMP radio occultation data, *Geophys. Res. Lett.*, *35*, L16807, doi:10.1029/2008GL034986.

Schwartz, M. J., et al. (2008), Validation of the Aura Microwave Limb Sounder temperature and geopotential height measurements, *J. Geophys. Res.*, D15S11, doi:10.1029/2007JD008783.

Shibata, T., K. Sato, H. Kobayashi, M. Yabuki, and M. Shiobara (2003), Antarctic polar stratospheric clouds under temperature perturbation by nonorographic inertia gravity waves observed by micropulse lidar at Syowa Station, *J. Geophys. Res.*, *108*(D3), 4105, doi:10.1029/2002JD002713.

Swinbank, R., and A. O'Neill (1994), A stratosphere-troposphere data assimilation system, *Mon. Weather Rev.*, *122*, 686–702.

Tabazadeh, A., E. J. Jensen, O. B. Toon, K. Drdla, and M. R. Schoeberl (2001), Role of the stratospheric polar freezing belt in denitrification, *Science*, *291*, 2591–2594.

Teitelbaum, H., and R. Sadourny (1998), The role of planetary waves in the formation of polar stratospheric clouds, *Tellus, Ser. A*, *50*, 302–312.

Vincent, R. A., A. Hertzog, G. Boccara, and F. Vial (2007), Quasi-Lagrangian superpressure balloon measurements of gravity wave momentum fluxes in the polar stratosphere of both hemispheres, *Geophys. Res. Lett.*, *34*, L19804, doi:10.1029/2007GL031072.

Watanabe, S., K. Sato, and M. Takahashi (2006), A general circulation model study of the orographic gravity waves over Antarctica excited by katabatic winds, *J. Geophys. Res.*, *111*, D18104, doi:10.1029/2005JD006851.

Waters, J. W., et al. (2006), The Earth Observing System Microwave Limb Sounder (EOS MLS) on the Aura satellite, *IEEE Trans. Geosci. Remote Sens.*, *44*, 1075–1092.

Winker, D. M., W. H. Hunt, and M. J. McGill (2007), Initial performance assessment of CALIOP, *Geophys. Res. Lett.*, *34*, L19803, doi:10.1029/2007GL030135.

World Meteorological Organization (2007), Scientific assessment of ozone depletion: 2006 global ozone research and monitoring project, *Rep. 50*, 572 pp., Geneva, Switzerland.

Wu, D. L., and J. H. Jiang (2002), MLS observations of atmospheric gravity waves over Antarctica, *J. Geophys. Res.*, *107*(D24), 4773, doi:10.1029/2002JD002390.

Wu, D. L., and J. W. Waters (1996), Satellite observations of atmospheric variances: A possible indication of gravity waves, *Geophys. Res. Lett.*, *23*, 3631–3634.

Zondlo, M. A., P. K. Hudson, A. J. Prenni, and M. A. Tolbert (2000), Chemistry and microphysics of polar stratospheric clouds and cirrus clouds, *Ann. Rev. Phys. Chem.*, *51*, 473–499.

S. P. Alexander and A. R. Klekociuk, Australian Antarctic Division, 203 Channel Hwy., Kingston, Tas 7050, Australia. (simon.alexander@aad.gov.au)

A. Arevalo-Torres and A. J. McDonald, Department of Physics and Astronomy, University of Canterbury, Christchurch 8020, New Zealand.

M. C. Pitts, NASA Langley Research Center, Hampton, VA 23681, USA.